JACS
JOURNAL OF THE AMERICAN CHEMICAL SOCIETY
Communication
pubs.acs.org/JACS

Controlled Synthesis of Highly Crystalline MoS_2 Flakes by Chemical Vapor Deposition

Xinsheng Wang, Hongbin Feng, Yongmin Wu, and Liying Jiao*

Key Lab of Organic Optoelectronics & Molecular Engineering, Department of Chemistry, Tsinghua University, Beijing 100084, China

Supporting Information

ABSTRACT: The controlled synthesis of highly crystalline MoS_2 atomic layers remains a challenge for the practical applications of this emerging material. Here, we developed an approach for synthesizing MoS_2 flakes in rhomboid shape with controlled number of layers by the layer-by-layer sulfurization of MoO_2 microcrystals. The obtained MoS_2 flakes showed high crystallinity with crystal domain size of ~10 μm, significantly larger than the grain size of MoS_2 grown by other methods. As a result of the high crystallinity, the performance of back-gated field effect transistors (FETs) made on these MoS_2 flakes was comparable to that of FETs based on mechanically exfoliated flakes. This simple approach opens up a new avenue for controlled synthesis of MoS_2 atomic layers and will make this highly crystalline material easily accessible for fundamental aspects and various applications.

Semiconducting transition metal dichalcogenides, such as MoS_2, have recently emerged as a family of 2D materials that are complementary to zero-bandgap graphene.[1−4] The intrinsic large bandgap (1.2−1.8 eV) and flexibility of MoS_2 atomic layers allow for their applications in nanoelectronic and optoelectronic devices on both conventional and flexible substrates.[5−12] Top-gated transistors based on mechanically exfoliated single-layer MoS_2 flakes showed excellent on/off current ratio of ~10^8 and mobility of >200 $cm^2\ V^{-1}\ s^{-1}$.[5] Logic circuits based on MoS_2 flakes were also fabricated to demonstrate their integration versatility.[6,8] It is critical to produce high-quality MoS_2 thin films with controlled numbers of layers for the practical application of MoS_2 in electronics.[3] Recently, single- and few-layered MoS_2 have been made by both "top-down" exfoliation and "bottom-up" synthesis. Similar to graphene, atomically thin flakes of MoS_2 exfoliated by mechanical cleavage showed the highest quality, but the size of the flakes was small (a few micrometers), and their thickness and shape were not controllable.[3] Solution-phase production of MoS_2 by exfoliation[13,14] or hydrothermal synthesis[15,16] holds promise for large-scale production, but application of these materials in electronics is restricted by the low quality of MoS_2 thus made. Very recently, chemical vapor deposition (CVD), which was successful in growing high-quality graphene, has been utilized to synthesize MoS_2 thin films on insulating substrates, such as SiO_2 and sapphire.[17−20] However, it is more challenging to obtain crystalline MoS_2 thin film with controlled number of layers by CVD than graphene, because the geometry, thickness, and crystallinity of graphene could be well-controlled by suitable catalyst design,[21,22] but no catalyst is involved in the growth of MoS_2. Currently, to achieve 2D growth of MoS_2, precursors such as Mo,[20] MoO_3,[18] or $(NH_4)_2MoS_4$[17] were first deposited on substrates as thin films before the sulfurization or thermal decomposition of these precursors at elevated temperature to define the 2D geometry of MoS_2 product. Obviously, this strategy could produce large-area MoS_2 films, but the obtained films were polycrystalline with small crystal grain size as the result of noncrystalline precursors used and the number of layers was not controllable. So far, the largest single-crystal domain size of MoS_2 grown on insulating substrates by CVD was ~160 nm in diameter.[17,18,20] The grain boundaries in these polycrystalline films could greatly degrade the electrical performance of MoS_2. van der Waals epitaxy of MoS_2 hexagonal flakes on graphene[23] and physical vapor deposition of MoS_2[24] were capable of growing highly crystalline MoS_2 flakes, but the number of layers of MoS_2 could not be controlled. Thus far, a method capable of producing pristine MoS_2 atomic layers in a controlled manner is still lacking.

Here we present a new approach for the growth of highly crystalline MoS_2 flakes with controlled number of layers by using MoO_2 microcrystals as templates. The synthesis strategy of MoS_2 flakes is schematically illustrated in Figure 1a. Briefly, MoO_3 powder was thermally evaporated and reduced by sulfur vapor in gas phase at 650−850 °C, and then the resulting MoO_2 was nucleated on SiO_2/Si substrates and grew up to rhomboidal microplates in a CVD furnace (see the setup in Supporting Information Figure S1). The MoO_2 microplates were then annealed in sulfur vapor carried by Ar at 850−950 °C for 0.5−6 h. During the high-temperature annealing, the surface of MoO_2 microplates was sulfurized to MoS_2 with varied numbers of layers depending on the annealing duration. After that, a PMMA thin film was spin-coated on the MoS_2/MoO_2 microplates to peel-off MoS_2 thin layers from MoO_2 and transfer them onto other substrates using PMMA-mediated nanotransfer printing.[25]

Optical images of as-made MoS_2/MoO_2 plates synthesized by reducing MoO_3 at 650 °C and then annealing at 850 °C for 3 h, the cleaved MoS_2 flakes, and the MoO_2 plates left on the growth substrate (Figures 1b,c, and S2a) demonstrate successful separation of MoS_2 from MoO_2. The rhomboidal shape of MoS_2 was well-maintained after the transfer, as shown in the optical images and scanning electron microscopy (SEM)

Received: February 5, 2013
Published: March 14, 2013

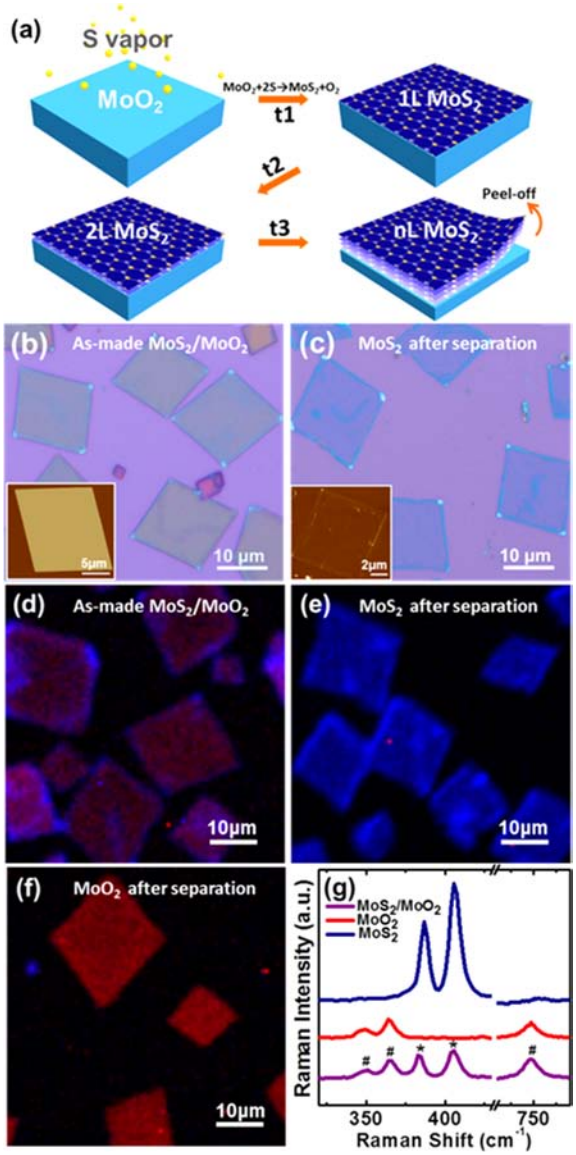

Figure 1. Synthesis and cleavage of MoS_2. (a) Schematics for the synthesis and cleavage of MoS_2. MoO_2 microplates were synthesized by reduction of MoO_3 and then used as template to grow MoS_2 by layer-by-layer surface sulfurization. The obtained MoS_2 coating was separated from MoO_2 and transferred to another substrate with the top layer facing up for further characterizations. 1L, 2L, and *n*L indicate single layer, bilayer, and *n*-layer, respectively. For simplicity, the growth of MoS_2 on the four sides of MoO_2 was not shown in this schematic. (b,c) Optical and AFM (insets) images of as-made MoS_2/MoO_2 plates grown by annealing in sulfur vapor for 3 h and the transferred MoS_2 flakes, respectively. Section analysis of AFM images was shown in Figure S2e,f. (d−f) Raman mapping images of as-made MoS_2/MoO_2, separated MoS_2, and MoO_2 with ∼405 cm^{-1} (assigned to MoS_2, blue) and ∼748 cm^{-1} (assigned to MoO_2, red) peak intensities using 514 nm laser excitation. (g) Typical Raman spectra of MoS_2/MoO_2 microplates, separated MoS_2, and MoO_2, respectively. Peaks marked with ∗ and # correspond to MoS_2 and MoO_2, respectively. The upshift of E^1_{2g} and A_{1g} modes after the transfer may indicate that the as-grown MoS_2 undergoes tensile strain on MoO_2 and the strain is released after the separation of MoS_2 from MoO_2 (Figure S3).

images (Figure S2c,d). The length of most MoS_2 flakes was ∼5−20 μm (Figure S2b), obviously larger than irregular MoS_2 flakes obtained by mechanical or chemical exfoliation of MoS_2 crystals. The thickness of the obtained MoS_2 flake measured by AFM was ∼1.5 nm (assigned to bilayer;[26] single-layer MoS_2 flakes with thickness of ∼0.8 nm were occasionally observed), significantly thinner than the as-made MoS_2/MoO_2 plates (∼120 nm, insets of Figures 1b,c and S2e,f), suggesting that only the outmost MoO_2 was sulfurized. Raman spectroscopy was used to further confirm the complete separation of MoS_2 from MoO_2. The as-made MoS_2/MoO_2 plates showed five Raman peaks in the range of 300−800 cm^{-1} under 514 nm excitation assigned to MoS_2 (E^1_{2g} mode ∼384 cm^{-1} and A_{1g} mode ∼405 cm^{-1})[26,27] and MoO_2 (∼350, 365, and 748 cm^{-1}).[28] After the separation, MoS_2 flakes did not show any peaks from MoO_2 and vice versa (Figure 1g). Figure 1d−f shows Raman mapping images with ∼405 cm^{-1} (strongest peak of MoS_2, blue) and ∼748 cm^{-1} (strongest peak of MoO_2, red) peak intensities collected on as-made MoS_2/MoO_2, separated MoS_2, and MoO_2, respectively. The mapping images of MoS_2 and MoO_2 after separation show pure colors of blue and red, respectively, further confirming that MoS_2 and MoO_2 were separated exactly at their interface.

X-ray photoelectron spectroscopy (XPS) and X-ray diffraction (XRD) were used to study the elemental composition and crystal structure of the products. The Mo 3d orbit of transferred MoS_2 flakes showed two peaks at 229.6 and 232.7 eV, which were attributed to the doublet of Mo $3d_{5/2}$ and Mo $3d_{3/2}$, respectively (Figure S4a). The binding energies for S $2p_{3/2}$ and $2p_{1/2}$ were 162.5 and 163.7 eV, respectively (Figure S4b). These measured binding energies agreed well with MoS_2 crystals with hexagonal symmetry.[29] The atomic ratio of Mo and S estimated from XPS is ∼1:2, further confirming the formation of MoS_2. XRD patterns of the MoS_2/MoO_2 microplates were accordance with monoclinic MoO_2 (P21) (ICDD card no: 76-1807) and hexagonal MoS_2 (P63) (ICDD card no: 77-1716) (Figure S4c), suggesting that the crystal structure changed, accompanied with the replacement of O atoms with S atoms.

We utilized transmission electron microscopy (TEM) to investigate the structures of MoS_2 flakes in details. Figure 2a shows a typical TEM image of MoS_2 flakes grown by 3 h annealing. To identify the number of layers in this sample, we imaged the folded edges occasionally found on the holey carbon grid and observed two parallel dark lines with a spacing of ∼6.5 Å, confirming that the MoS_2 flakes were bilayers as estimated by AFM. Figure 2b displays the selected area electron diffraction (SAED) pattern taken on the bilayer MoS_2 flake with an aperture size of ∼3.8 μm (inset of Figure 2b), showing hexagonal symmetry for the MoS_2 structure. We also collected SAED patterns at multiple locations on this flake and obtained hexagonal patterns with the same orientations, indicating the lateral crystal domain size of this MoS_2 flake was >10 μm (Figure S5), comparable to that of exfoliated MoS_2 flakes[20] and significantly larger than the domain size of MoS_2 grown on insulating substrates by other CVD methods (∼160 nm).[17,18,20] High-resolution TEM image of the bilayer MoS_2 flake showed a honeycomb arrangement of the atoms with lattice spacing of 2.7 and 1.6 Å, corresponding to the (100) and (110) planes (Figure 2c).

The high crystallinity of the obtained MoS_2 flakes was attributed to the surface sulfurization of crystalline MoO_2 microplates. The well-ordered packing of Mo atoms on the surface of MoO_2 crystal determined that the resulting MoS_2 layers were still crystalline after O atoms were replaced with S atoms. This kind of surface sulfurization was similar to the

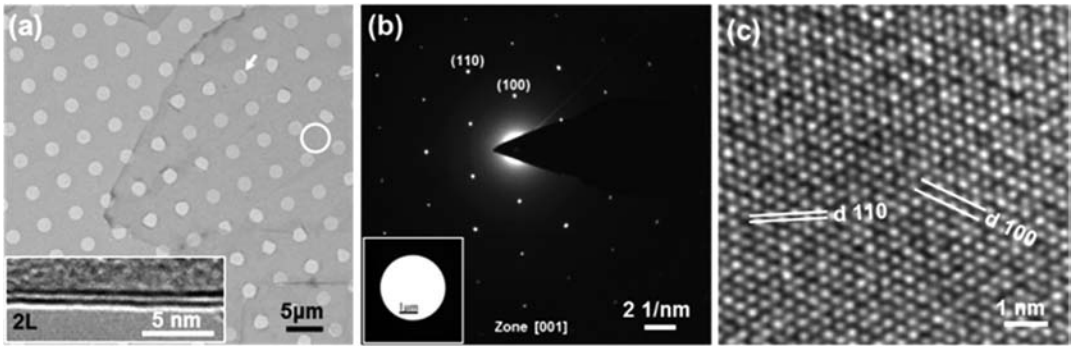

Figure 2. TEM characterizations of MoS_2 flakes. (a) Low-magnification TEM image of MoS_2 flakes supported on holey carbon grid. Inset: folded MoS_2 edge at the point marked with an arrow. The spacing between the two dark lines was ~6.5 Å, consistent with the layer spacing in hexagonal MoS_2 crystal. (b) SAED patterns taken on the area of MoS_2 flake marked in the circle in (a). Inset: TEM image of the marked area in (a) with the aperture. The diameter of the aperture was ~3.8 μm. (c) Enlarged high-resolution TEM image of MoS_2 showing hexagonal lattice.

sulfurization of MoO_2 nanoparticles, which was commonly used for synthesizing MoS_2 fullerene-like particles, and the mechanism has been intensely studied: During the sulfurization, the first few layers of the oxide particles were sulfurized quickly, followed by a slow, diffusion-controlled sulfurization leading to the complete conversion of oxide to sulfide layer-by-layer. The rate of sulfurization was limited by the rate of diffusion of sulfur atoms through the already existing MoS_2 outer walls and became slower with increasing number of MoS_2 layers.[30,31] Because the MoO_2 microplates were significantly larger and more crystalline than the MoO_2 nanoparticles, the surface sulfurization of MoO_2 microplates was expected to be much slower than that of nanoparticles. This slow, layer-by-layer sulfurization allowed for precisely controlling the thickness of MoS_2 by tuning the sulfurization time. Besides the bilayer flakes obtained by annealing for 3 h, MoS_2 flakes with thicknesses of ~0.8, ~0.8−1.4, and ~2.0−2.8 nm, corresponding to 1L, 1−2L, and 3−4L,[26] were synthesized by annealing for 0.5, 1, and 6 h, respectively (Figures 3a, S6a, and 3b, respectively). The MoS_2 samples with varied thickness were also investigated using Raman and photoluminescence (PL) spectroscopy. The frequency difference between A_{1g} mode and E^1_{2g} mode has been widely used for identifying the number of layers of MoS_2 thin film.[17,26] We measured the frequency difference on the transferred MoS_2 samples and estimated the number of layers for MoS_2 flakes obtained by annealing for 0.5, 1−3, and 6 h to be 1L, 1−2L and 4L, respectively, using mechanically exfoliated MoS_2 flakes as reference (Figure 3c).[26] These results were in agreement with the number of layers assigned by AFM measurements. The PL spectra of MoS_2 flakes exhibited two peaks at ~625 and 672 nm, corresponding to the A1 and B1 direct excitonic transitions, respectively.[27] Gradual increases in the PL intensities with annealing time also indicated that the thickness of MoS_2 increased with prolonged annealing (Figure 3d).[27,32] The control over layer numbers achieved by this surface sulfurization approach is significant to the fundamental studies and applications of MoS_2, because this material exhibits obvious layer-dependent band structure and properties.[3] We also investigated the effects of other parameters such as annealing temperature, reduction temperature, growth substrates, and additional metal oxides on the geometry and thickness of MoS_2 flakes (see discussions in Supporting Information, Figures S7−S10). The growth of rhomboidal MoS_2 flakes tolerated relatively broad variations in growth parameters.

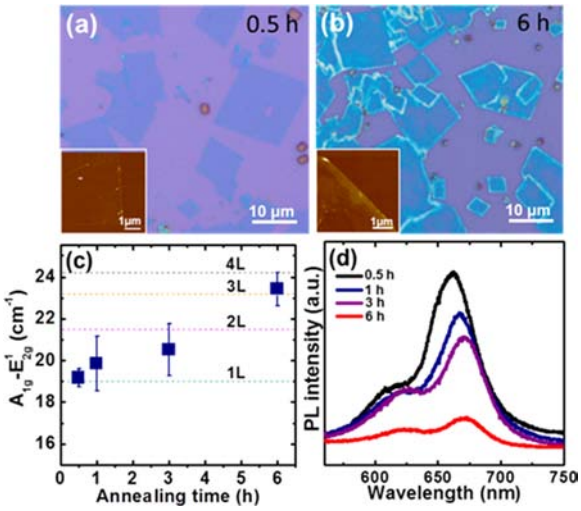

Figure 3. Thickness dependence of MoS_2 flakes with annealing time. (a,b) Optical and AFM (insets) images of transferred MoS_2 flakes synthesized by annealing for 0.5 and 6 h, respectively. (c) Frequency difference between A_{1g} and E^1_{2g} of transferred MoS_2 as a function of annealing time. The dashed lines labeled 1L to 4L were the averaged A_{1g}−E^1_{2g} measured on 1−4 layers mechanically exfoliated MoS_2. (d) PL spectra of MoS_2 obtained by annealing for varied duration.

The regular shape and size of a few to tens of micrometers of the MoS_2 flakes greatly facilitated the fabrication of MoS_2 field-effect transistor (FET) devices. We fabricated FETs with ~200 nm to 1.5 μm channel lengths on bilayer MoS_2 flakes using 10 nm Ti/50 nm Au as source and drain electrodes, 300-nm-thick SiO_2 as dielectrics and p^{++} Si as the back gate by electron beam lithography and electron beam deposition. The transfer characteristics of a bilayer MoS_2 flake measured at room temperature in atmosphere exhibited n-type conduction with an on/off current ratio of ~10^6 (Figure 4). The field-effect mobility of this MoS_2 FET was estimated to be ~0.3 cm^2 V^{-1} s^{-1}. The on/off current ratios and mobility of all 17 FETs we measured were in the ranges of 10^4−10^6 and 0.1−0.7 cm^2 V^{-1} s^{-1}, respectively (Figure S11), comparable with those of back-gated FETs made with mechanically exfoliated MoS_2 flakes (0.1−10 cm^2 V^{-1} s^{-1}).[1,3,7] The mobility of our MoS_2 FETs could be greatly improved by using Sc as source and drain electrodes and high-k top gate dielectrics, such as HfO_2 or Al_2O_3.[5,33]

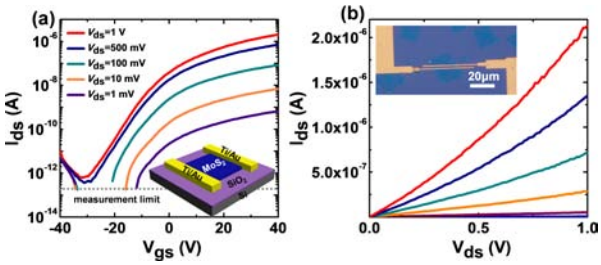

Figure 4. Electrical properties of devices made on a bilayer MoS_2 flake. (a) $I_{ds}-V_{gs}$ curves for the bilayer MoS_2 FET shown in the inset of (b) at various biases probed in air. Inset: schematic for the back-gated FET with a MoS_2 flake as channel. (b) $I_{ds}-V_{ds}$ curves for the device in (a) at varied V_{gs} from −40 to 40 V at steps of 10 V from bottom to top. The channel length and width of this FET were ∼1.1 and 20.0 μm, respectively. Inset: optical image of the device.

In summary, we present an approach for synthesizing MoS_2 atomic layers with controlled shape and number of layers by the layer-by-layer surface sulfurization of MoO_2 microplates. The obtained MoS_2 flakes exhibited rhomboidal shape with lengths up to tens of micrometers, obviously larger than irregular flakes exfoliated from MoS_2 crystals. These MoS_2 flakes exhibited high crystallinity with a crystal domain size of ∼10 μm and mobility comparable with that of mechanically exfoliated MoS_2 flakes. This simple and reliable approach opens up a new way for producing highly crystalline MoS_2 atomic layers in a controlled manner. The regular shape, large size, and controlled number of layers combined with high crystallinity of the MoS_2 flakes make them promising materials for applications in high-performance nanoelectronics and optoelectronics.

■ ASSOCIATED CONTENT

Ⓢ Supporting Information

Experimental details, microscopic and spectroscopic characterizations, XRD and XPS data, SAED patterns, effects of various parameters on the growth, and statistics on the performance of MoS_2 FETs. This material is available free of charge via the Internet at http://pubs.acs.org.

■ AUTHOR INFORMATION

Corresponding Author

lyjiao@mail.tsinghua.edu.cn

Notes

The authors declare no competing financial interest.

■ ACKNOWLEDGMENTS

This work was supported by National Program for Thousand Young Talents of China and Tsinghua-Foxconn Nanotechnology Research Center.

■ REFERENCES

(1) Novoselov, K. S.; Jiang, D.; Schedin, F.; Booth, T. J.; Khotkevich, V. V.; Morozov, S. V.; Geim, A. K. *Proc. Natl. Acad. Sci. U.S.A.* **2005**, *102*, 10451.
(2) Chen, D.; Tang, L. H.; Li, J. H. *Chem. Soc. Rev.* **2010**, *39*, 3157.
(3) Wang, Q. H.; Kalantar-Zadeh, K.; Kis, A.; Coleman, J. N.; Strano, M. S. *Nat. Nanotechnol.* **2012**, *7*, 699.
(4) Huang, X.; Zeng, Z. Y.; Zhang, H. *Chem. Soc. Rev.* **2013**, *42*, 1934.
(5) Radisavljevic, B.; Radenovic, A.; Brivio, J.; Giacometti, V.; Kis, A. *Nat. Nanotechnol.* **2011**, *6*, 147.
(6) Radisavljevic, B.; Whitwick, M. B.; Kis, A. *ACS Nano* **2011**, *5*, 9934.
(7) Yin, Z. Y.; Li, H.; Li, H.; Jiang, L.; Shi, Y. M.; Sun, Y. H.; Lu, G.; Zhang, Q.; Chen, X. D.; Zhang, H. *ACS Nano* **2012**, *6*, 74.
(8) Wang, H.; Yu, L. L.; Lee, Y. H.; Shi, Y. M.; Hsu, A.; Chin, M. L.; Li, L. J.; Dubey, M.; Kong, J.; Palacios, T. *Nano Lett.* **2012**, *12*, 4674.
(9) He, Q. Y.; Zeng, Z. Y.; Yin, Z. Y.; Li, H.; Wu, S. X.; Huang, X.; Zhang, H. *Small* **2012**, *8*, 2994.
(10) Liu, J. Q.; Zeng, Z. Y.; Cao, X. H.; Lu, G.; Wang, L. H.; Fan, Q. L.; Huang, W.; Zhang, H. *Small* **2012**, *8*, 3517.
(11) Li, H.; Yin, Z. Y.; He, Q. Y.; Li, H.; Huang, X.; Lu, G.; Fam, D. W. H.; Tok, A. I. Y.; Zhang, Q.; Zhang, H. *Small* **2012**, *8*, 63.
(12) Pu, J.; Yomogida, Y.; Liu, K. K.; Li, L. J.; Iwasa, Y.; Takenobu, T. *Nano Lett.* **2012**, *12*, 4013.
(13) Coleman, J. N.; Lotya, M.; O'Neill, A.; Bergin, S. D.; King, P. J.; Khan, U.; Young, K.; Gaucher, A.; De, S.; Smith, R. J.; Shvets, I. V.; Arora, S. K.; Stanton, G.; Kim, H. Y.; Lee, K.; Kim, G. T.; Duesberg, G. S.; Hallam, T.; Boland, J. J.; Wang, J. J.; Donegan, J. F.; Grunlan, J. C.; Moriarty, G.; Shmeliov, A.; Nicholls, R. J.; Perkins, J. M.; Grieveson, E. M.; Theuwissen, K.; McComb, D. W.; Nellist, P. D.; Nicolosi, V. *Science* **2011**, *331*, 568.
(14) Zeng, Z. Y.; Yin, Z. Y.; Huang, X.; Li, H.; He, Q. Y.; Lu, G.; Boey, F.; Zhang, H. *Angew. Chem., Int. Ed.* **2011**, *50*, 11093.
(15) Peng, Y. Y.; Meng, Z. Y.; Zhong, C.; Lu, J.; Yu, W. C.; Jia, Y. B.; Qian, Y. T. *Chem. Lett.* **2001**, *30*, 772.
(16) Matte, H. S. S. R.; Gomathi, A.; Manna, A. K.; Late, D. J.; Datta, R.; Pati, S. K.; Rao, C. N. R. *Angew. Chem., Int. Ed.* **2010**, *49*, 4059.
(17) Liu, K. K.; Zhang, W. J.; Lee, Y. H.; Lin, Y. C.; Chang, M. T.; Su, C.; Chang, C. S.; Li, H.; Shi, Y. M.; Zhang, H.; Lai, C. S.; Li, L. J. *Nano Lett.* **2012**, *12*, 1538.
(18) Lin, Y. C.; Zhang, W. J.; Huang, J. K.; Liu, K. K.; Lee, Y. H.; Liang, C. T.; Chu, C. W.; Li, L. J. *Nanoscale* **2012**, *4*, 6637.
(19) Lee, Y. H.; Zhang, X. Q.; Zhang, W. J.; Chang, M. T.; Lin, C. T.; Chang, K. D.; Yu, Y. C.; Wang, J. T. W.; Chang, C. S.; Li, L. J.; Lin, T. W. *Adv. Mater.* **2012**, *24*, 2320.
(20) Zhan, Y. J.; Liu, Z.; Najmaei, S.; Ajayan, P. M.; Lou, J. *Small* **2012**, *8*, 966.
(21) Dai, B. Y.; Fu, L.; Zou, Z. Y.; Wang, M.; Xu, H. T.; Wang, S.; Liu, Z. F. *Nat. Commun.* **2011**, *2*, 522.
(22) Ago, H.; Ito, Y.; Mizuta, N.; Yoshida, K.; Hu, B.; Orofeo, C. M.; Tsuji, M.; Ikeda, K.; Mizuno, S. *ACS Nano* **2010**, *4*, 7407.
(23) Shi, Y. M.; Zhou, W.; Lu, A. Y.; Fang, W. J.; Lee, Y. H.; Hsu, A. L.; Kim, S. M.; Kim, K. K.; Yang, H. Y.; Li, L. J.; Idrobo, J. C.; Kong, J. *Nano Lett.* **2012**, *12*, 2784.
(24) Wu, S.; Huang, C.; Aivazian, G.; Ross, J. S.; Cobden, D. H.; Xu, X. *ACS Nano* **2013**, DOI: 10.1021/nn4002038.
(25) Jiao, L. Y.; Fan, B.; Xian, X. J.; Wu, Z. Y.; Zhang, J.; Liu, Z. F. *J. Am. Chem. Soc.* **2008**, *130*, 12612.
(26) Lee, C.; Yan, H.; Brus, L. E.; Heinz, T. F.; Hone, J.; Ryu, S. *ACS Nano* **2010**, *4*, 2695.
(27) Li, H.; Zhang, Q.; Yap, C. C. R.; Tay, B. K.; Edwin, T. H. T.; Olivier, A.; Baillargeat, D. *Adv. Funct. Mater.* **2012**, *22*, 1385.
(28) Dieterle, M.; Mestl, G. *Phys. Chem. Chem. Phys.* **2002**, *4*, 822.
(29) Baker, M. A.; Gilmore, R.; Lenardi, C.; Gissler, W. *Appl. Surf. Sci.* **1999**, *150*, 255.
(30) Feldman, Y.; Wasserman, E.; Srolovitz, D. J.; Tenne, R. *Science* **1995**, *267*, 222.
(31) Rosentsveig, R.; Margolin, A.; Gorodnev, A.; Popovitz-Biro, R.; Feldman, Y.; Rapoport, L.; Novema, Y.; Naveh, G.; Tenne, R. *J. Mater. Chem.* **2009**, *19*, 4368.
(32) Eda, G.; Yamaguchi, H.; Voiry, D.; Fujita, T.; Chen, M. W.; Chhowalla, M. *Nano Lett.* **2011**, *11*, 5111.
(33) Das, S.; Chen, Y.-H.; Penumatcha, A. V.; Appenzeller, J. *Nano Lett.* **2013**, *1*, 100.